Environmental Science & Technology

ARTICLE

pubs.acs.org/est

# Measurements of Nitrous Acid in Commercial Aircraft Exhaust at the Alternative Aviation Fuel Experiment

Ben H. Lee,*[,†] Gregory W. Santoni,[†] Ezra C. Wood,[‡,§] Scott C. Herndon,[‡] Richard C. Miake-Lye,[‡] Mark S. Zahniser, Steven C. Wofsy,[†] and J. William Munger[†]

[†]Harvard University, Cambridge, MA 02138, United States

[‡]Aerodyne Research, Inc., Billerica, MA 01821, United States

Supporting Information

**ABSTRACT:** The Alternative Aviation Fuel Experiment (AAFEX), conducted in January of 2009 in Palmdale, California, quantified aerosol and gaseous emissions from a DC-8 aircraft equipped with CFM56-2C1 engines using both traditional and synthetic fuels. This study examines the emissions of nitrous acid (HONO) and nitrogen oxides ($NO_x = NO + NO_2$) measured 145 m behind the grounded aircraft. The fuel-based emission index (EI) for HONO increases approximately 6-fold from idle to takeoff conditions but plateaus between 65 and 100% of maximum rated engine thrust, while the EI for $NO_x$ increases continuously. At high engine power, $NO_x$ EI is greater when combusting traditional (JP-8) rather than Fischer−Tropsch fuels, while HONO exhibits the opposite trend. Additionally, hydrogen peroxide ($H_2O_2$) was identified in exhaust plumes emitted only during engine idle. Chemical reactions responsible for emissions and comparison to previous measurement studies are discussed.

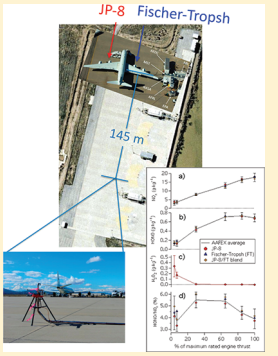


## 1. INTRODUCTION

The effects of aircraft exhaust on air quality and climate are a growing concern given the projected global increase in air travel over the coming decades. Uncertainties associated with induced indirect effects related to microphysical processes and heterogeneous chemistry have been the focus of numerous previous studies,[1−4] which stress among others the importance of characterizing emissions and their driving factors to evaluate the influence of the aviation transportation sector on chemistry, radiative forcing and public health.

Nitrous acid (HONO) is the primary reservoir of hydroxyl radicals (OH) emitted in fresh jet exhaust.[5,6] HONO during daytime undergoes rapid photolysis, yielding OH, which initiates the oxidation of simultaneously emitted nitrogen oxides ($NO_x = NO + NO_2$), sulfur dioxide ($SO_2$), and volatile organic compounds (VOCs). Heterogeneous chemistry on the surface of aircraft-generated particles can further shift the partitioning of in-plume $NO_x$ toward $NO_y$ ($=NO_x + HNO_3 + HONO + ...$), altering the impact of emission on ozone ($O_3$) levels at altitude.[7] Moreover, enhanced reactivity in exhaust from idling and taxiing aircraft adversely affects air quality in and around airports.[8] HONO itself is a lung irritant and reacts with amines to form carcinogenic compounds.[9−11]

Fischer−Tropsch (FT) fuels, despite high energy costs of production, have gained much attention as a viable alternative to imported oil because the main feedstocks are readily available (e.g., coal, natural gas, and bio-oils). In addition, FT-derived fuels do not contain aromatic-hydrocarbon and sulfur compounds, resulting in emissions that are typically lower in soot and sulfate aerosols. A recent study observed lower NO and higher $NO_2$ emissions in FT-derived exhaust compared to those combusting traditional JP-8 fuel.[12] Simultaneous measurements of $NO_x$ and HONO during the Alternative Aviation Fuel Experiment (AAFEX) provided an opportunity to further investigate fuel-type dependence of nitrogen oxide emissions from jet engines. We present fuel-based emission indices of HONO, $NO_x$, and hydrogen peroxide ($H_2O_2$) emitted from CFM56-2C1 commercial aircraft engines as a function of engine power.

## 2. METHODS

During AAFEX, a DC-8 was chocked on the runway at NASA's Dryden Aircraft Operation Facility in Palmdale, California. Two of its four engines (one on each side) were fired for 12 experiments, each typically lasting a few hours, during which the rated engine thrust was varied to simulate idle to takeoff conditions. The left (control) inboard engine was supplied with traditional JP-8 fuel, while the right (experiment) alternated between traditional, two different Fischer−Tropsch fuels and blends of both. JP-8 fuel, utilized by the military, contains additives to enhance lubrication/inhibit icing that are not present in Jet A-1 fuel, most commonly used in commercial aviation, but exhibit similar combustion emission properties.[13] Experiments were conducted from before sunrise to late afternoon over a span of eight

Received: March 18, 2011
Accepted: August 2, 2011
Revised: July 26, 2011
Published: August 02, 2011

**Table 1. Fuel Used, Average Ambient Temperature, and Relative Humidity for Each Experiment during AAFEX**

| experiment no. | date | fuel[a] | ambient temperature (°C) | relative humidity (%) |
|---|---|---|---|---|
| 1 | Jan. 26 | JP-8 | 5 | 60 |
| 2 | Jan. 27 | JP-8 | 10 | 30 |
| 3 | Jan. 28 | JP-8 | −3 | 30 |
| 4 | Jan. 28 | FT1 | 10 | 30 |
| 5 | Jan. 29 | FT1 | 0 | 60 |
| 6 | Jan. 30 | FT1[b] | 2 | 55 |
| 7 | Jan. 30 | FT2 | 14 | 25 |
| 8 | Jan. 31 | FT2 | 0 | 75 |
| 9 | Jan. 31 | FT2[b] | 14 | 30 |
| 10 | Jan. 31 | JP-8 | 17 | 20 |
| 11 | Feb. 2 | JP-8 | 2 | 60 |
| 12 | Feb. 2 | JP-8 | 12 | 25 |

[a] Fuel utilized by the right inboard engine. The left inboard engine powered by JP-8 for all experiments. FT1 derived from natural gas. FT2 derived from coal. [b] Right inboard engine fueled with 50/50 mixture by volume of JP-8/FT blend.

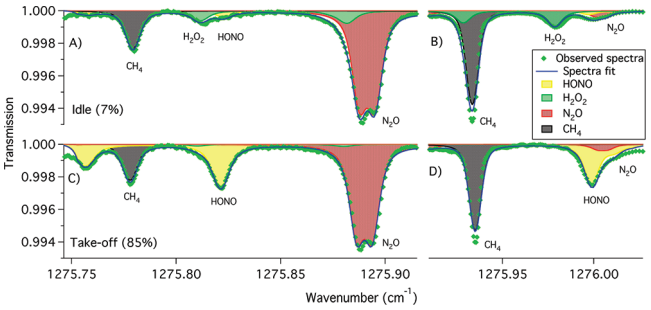


**Figure 1.** One-second spectra observed in aircraft exhaust emitted during 7% (a, b) and 85% (c, d) rated engine thrust. The above snapshots at idle and takeoff conditions represent $CH_4$, $N_2O$, HONO, and $H_2O_2$ values of 2000, 335, 10, 35 ppb and 1875, 325, 75, 5 ppb, respectively. For most of AAFEX, the spectral window shown in (a) and (c) was scanned, save for one day (experiment nos. 11 and 12) when the window in (b) and (d) was scanned. The filled-in color areas are simulations of the retrieved mixing ratios.

days to test the impact of the wide range in ambient conditions on emission characteristics. Composition and mixing ratios of particles and various trace gases were measured 1 and 30 m behind both engines and at a distance of 145 m in-line with the right inboard engine relative to the direction of the aircraft. This downstream location observed a mixture of naturally diluted and cooled exhaust from both engines and is the focus of the present study. Table 1 lists a brief description of the experimental conditions, with fuller details given by Bulzan et al.[14]

Mixing ratios of HONO, $H_2O_2$, nitrous oxide ($N_2O$), and methane ($CH_4$) were measured simultaneously by a tunable infrared laser differential absorption spectrometer (TILDAS) utilizing a continuous-wave quantum cascade laser (Alpes Lasers) operating near the 8 $\mu$m (1275 $cm^{-1}$) spectral region. Infrared light from the laser is directed into a multipass sample cell where the laser light reflects 238 times between two astigmatic high-reflectivity ($R = 0.993$) mirrors spaced 0.88 m apart to achieve a total absorption path length of 210 m. Light exits the sample cell and is directed onto a cryogenically cooled HgCdTe detector (Vigo). An absorbance precision less than $6 \times 10^{-6}$ $Hz^{-1/2}$ in one second was achieved in the field, which translated to detection limits ($S/N = 3$) of 450 ppt (pmol/mol), 1200 and 900 ppt for HONO, $H_2O_2$ and $N_2O$, respectively, in one second. Figure 1 shows typical one-second spectra observed while sampling plumes emitted during 7% (Figure 1a, b) and 85% (Figure 1c, d) of maximum rated engine thrust.

Special attention was paid to the sample handling to minimize HONO loss and artifact formation on instrument surfaces. Sample air, a variable mixture of exhaust and background air, was continuously pulled through a quartz inlet (length approximately 6 in. (15.2 cm); inner diameter approximately 0.25 in. (6.4 mm)), which was treated with siloxyl coating and shielded from sunlight to reduce surface chemistry. The sample subsequently passed through a critical orifice (0.04 in. diameter (1.0 mm)), to accelerate the flow and reduce the pressure, then diverged in two paths: a vent-flow parallel and sample-flow perpendicular to the direction of flow through the orifice. Inertial separation prevented coarse particles with diameters greater than about 4 $\mu$m from entering the sample cell.[15] This design was utilized instead of a particle filter, which would present a large surface area where loss or production of "sticky" gases could occur. The sample then traveled through approximately 40 feet (12.2 m) of $^3/_8$ in. (9.5 mm) outer diameter PFA tubing to the siloxyl-coated multipass sample cell in which the pressure was maintained at approximately 30 Torr. With a total flow rate of about 10 standard liters per minute (SLPM) the sample residence times (1/e) in the inlet, tubing, and cell were on average 0.3, 0.2, and 1.2 s, respectively. Additional details regarding the instrumentation and sampling schemes are provided elsewhere.[15] Results for $N_2O$ and $CH_4$, measured by a second TILDAS instrument connected in series with this system, are presented by Santoni et al.[16]

Introduction of air infused with HONO and $CH_4$ at the end of the eight day campaign showed indistinguishable response times between the two gases (Supporting Information, Figure S1), indicating no reversible loss of HONO on the inlet/tubing/cell surfaces. Laboratory tests prior to deployment that compared the signal of HONO standard introduced through the sampling inlet/tubing to the signal when HONO was introduced directly into the cell demonstrated no detectable loss of HONO on inlet/tubing walls. However, the same addition tests under field conditions could not be repeated during the experiments. Similar tests for $H_2O_2$ were not conducted because a steady source was not available in the field. Though the reduced pressure in the sample line and use of hydrophobic siloxyl coating minimize water activity on surfaces, we cannot discount the potential for loss of $H_2O_2$ given that the Henry's law constant for $H_2O_2$ is 82 000 M $atm^{-1}$ compared to 50 M $atm^{-1}$ for HONO.[17,18] In addition, spectral overlap between HONO and $H_2O_2$ absorption lines around 1275.82 $cm^{-1}$ (Figure 1a, c) during experiments 1−10 (Table 1) resulted in artificial enhancement of the retrieved $H_2O_2$ mixing ratios in the presence of high HONO. This was not observed when $H_2O_2$ was scanned near the 1275.98 $cm^{-1}$ region (Figure 1b, d), where its absorption lines were free of overlap. As a result, $H_2O_2$ data from only experiments 11 and 12 are reported. In-field additions of high levels of $H_2O_2$ showed no significant influence by $H_2O_2$ on calculated HONO mixing ratios.

Calibrations with a constant HONO source were not possible in the field. Instead, measurements relied on the accuracy of

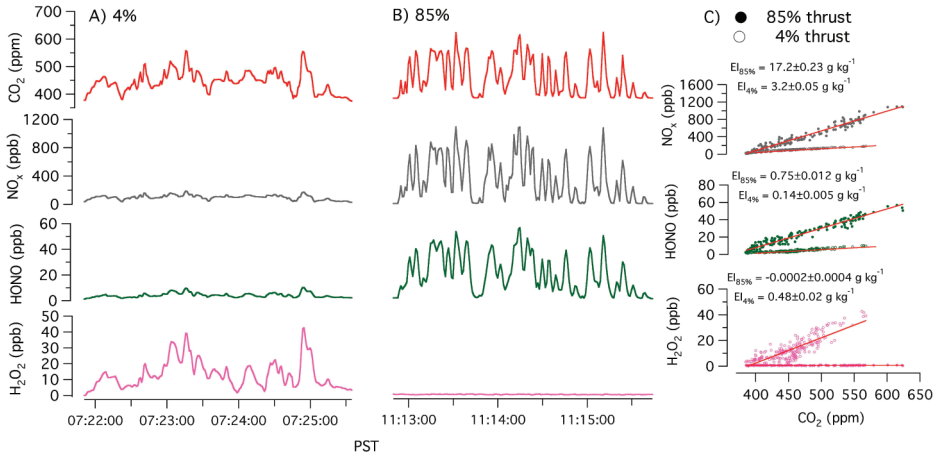


**Figure 2.** Mixing ratios of $CO_2$, $NO_x$, HONO, and $H_2O_2$ measured 145 m downwind of the aircraft in plumes emitted during 4% (a) and 85% (b) rated engine thrust. Correlation plots (c) of $NO_x$, HONO, and $H_2O_2$ versus $CO_2$ for the same time periods from (a) and (b), along with corresponding emission indices and standard errors.

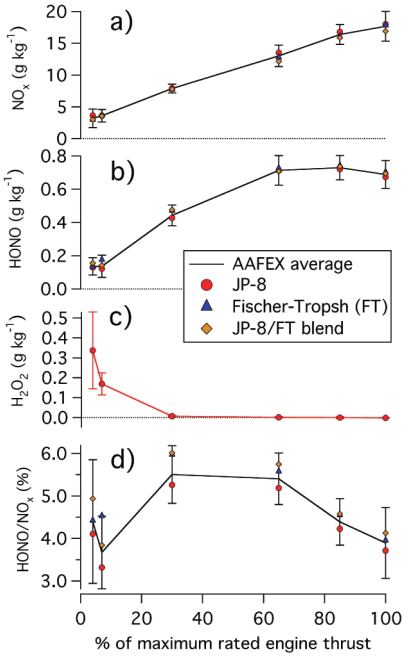


**Figure 3.** Emission indices (EI = g per kg of fuel) of $NO_x$ (a), HONO (b), and $H_2O_2$ (c) plotted against % of maximum rated engine thrust, along with HONO to $NO_x$ ratio (d). Each symbol represents the fuel-experiment average while the black trace is the campaign average ± one standard deviation of the mean at each engine power, except for (c), which shows results for JP-8 fuel experiments 11 and 12 only.

absorption line strengths. Line positions and relative line strengths for HONO were initially obtained from high-resolution FTIR spectra provided by Herman et al.[19−21] Absolute values were derived in the laboratory by measuring the absorbance of a high-purity HONO source with the TILDAS system. Total HONO in the generated source was simultaneously converted via molybdenum (Mo) catalysis to NO followed by quantification with a second calibrated TILDAS system.[22] We found that the previous aircraft emission study by Wood et al.[23] used incorrect line strength values that resulted in measurements of HONO to be low by a factor of approximately 2.4 (discussed below). Absorption parameters for $H_2O_2$, $CH_4$, and $N_2O$ are obtained from the HITRAN database.[24]

The $NO_x$ mixing ratio, the sum of NO and $NO_2$, was measured using Mo-catalysis ozone chemiluminescence (ThermoElectron 42i). The Mo catalyst converts other species besides $NO_2$, but because the converter was preceded by a particle filter and 40 ft of tubing maintained near ambient pressure, it is unlikely that reducible $NO_y$ species such as HONO and $HNO_3$ were transmitted. Mixing ratios of $CO_2$ were measured using a nondispersive infrared absorption spectrometer (Li-Cor 6262). The flow rate was approximately 0.5 SLPM for each of these two instruments connected in parallel to tubing dedicated to $NO_x$ and $CO_2$ measurements, resulting in sample residence times (1/e) of less than one second in each instrument.

To derive emission indices we compute slopes from linear regression of each species against $CO_2$ and convert to a fuel-based emission index (g of species per kg of fuel consumed) by scaling with the emission index for $CO_2$ (carbon content of the fuel). Regression slopes provide a more robust estimate of EI, with associated uncertainty, in downwind plumes with highly variable mixing ratios than the background-subtracted ratio of the average mixing ratio to $CO_2$.[25] Note that the EI for HONO and $H_2O_2$ are scaled by their respective molecular masses, while EI for $NO_x$ is reported using the molecular mass of $NO_2$:

$$\mathrm{EI}_x = m_{x,\mathrm{CO}_2} \times \frac{M_x}{M_{\mathrm{CO}_2}} \times \mathrm{EI}_{\mathrm{CO}_2}$$

where $\mathrm{EI}_x$ is the emission index of species $x$ (g of $x$ per kg fuel), $m_{x,\mathrm{CO}_2}$ is the slope of the linear regression between species $x$ and $CO_2$, $M$ is molecular weight (g of $x$ per mole of $x$), and $\mathrm{EI}_{\mathrm{CO}_2}$ is grams of $CO_2$ emitted per kilograms of fuel consumed determined for each fuel-type by C/H fuel analysis.[14] The analyses presented here utilize a single $\mathrm{EI}_{\mathrm{CO}_2}$ value for all experiments because the extent of mixing of exhaust from the two engines was unknown.

Figure 2(a, b) shows a brief 1 Hz time-series of HONO, $NO_x$, $H_2O_2$, and $CO_2$ mixing ratios. All gases covary in time. This is also reflected in the correlation of that same plume of HONO, $NO_x$, and $H_2O_2$ versus $CO_2$ mixing ratio (Figure 2c). The mean uncertainty in the emission indices, determined as the standard

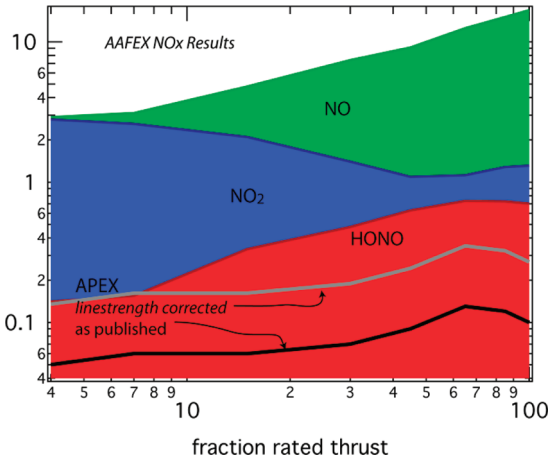


**Figure 4.** Emission index of HONO observed during the APEX-3 (black line). Revised APEX-3 values (gray line) using corrected line strength values overlaid on top of observations from AAFEX (red). Emission indices for $NO_2$ (blue) and NO (green) from APEX-3 are shown as well.

error of the regressed slopes, for HONO, $NO_x$, and $H_2O_2$ are 0.03, 0.4, and 0.01 g $kg^{-1}$, respectively, which are about a factor of 3 less than the observed plume-to-plume variability as seen in Figure 3.

## 3. RESULTS AND DISCUSSION

**3.1. HONO and $NO_x$ EI—Chemistry and Fuel Dependence.** Figure 3(a, b) shows the emission indices for $NO_x$ and HONO plotted as a function of the percentage of maximum rated engine thrust. The EI for $NO_x$, driven primarily by the Zeldovich reactions,[26] increases continuously with engine thrust, hence gas temperature during combustion. The EI for HONO in comparison levels off between 65 and 100% engine setting, an unexpected trend assuming OH production, presumably from the reaction between water vapor and $O(^1D)$ in the combustor, also increases continuously with engine power. Thermal decomposition ($R_{-1}$) alone may explain the flattening of HONO EI above 65% of rated engine thrust as proposed by Wood et al.; however, that HONO production is also underestimated at low engine power points to missing reactions and/or inaccurate kinetic constants.[23] Notably, published values for HONO self-reaction rate (R4) differ by 6 orders of magnitude:[27]

$$NO + OH + M \leftrightarrow HONO + M \quad (R_1)$$

$$NO_2 + HO_2 \rightarrow HONO + OH \quad (R_2)$$

$$HONO + OH \rightarrow H_2O + NO_2 \quad (R_3)$$

$$HONO + HONO \rightarrow H_2O + NO + NO_2 \quad (R_4)$$

Ab initio calculation by Xia and Lin of reaction rate R3 reveals a change from negative to positive temperature dependence above 1000 K,[28] which is consistent with our observed trend in HONO EI as the rate of HONO loss by OH becomes significant with increasing combustion temperature and OH levels. Though targeted measurements of $NO_2$, the product of reaction R3, were not made during AAFEX, results from a previous campaign Aircraft Particle Experiment-3 (APEX-3) show an increase in $NO_2$ EI at high engine power (Figure 4). Underestimation of reaction R3 in previous studies may also help reconcile the large discrepancy between engine exit OH levels predicted at cruise (9.0−13.2 ppm) [6] and observed under takeoff conditions (90 ppb).[29] Self-reaction of OH is ruled out because modeling studies[6,30] report near-complete titration of OH by excess NO and because this reaction would result in the production of $H_2O_2$, which was not observed at high engine power (discussed below). Heterogeneous chemistry, as well, plays a small role.[31]

**Table 2. $NO_x$ and HONO Emission Indices for FT and Blended Fuel Experiments Normalized by Those for JP-8**

| emission | fuel | 4% (low) | 7% (idle) | 30% (approach) | 65% (cruise) | 85% (climb-out) | 100% (takeoff) |
|---|---|---|---|---|---|---|---|
| $NO_x$ | FT | 0.82 | 1.03 | 0.97 | 0.95 | 0.96 | 0.99 |
| | blend | 0.83 | 0.99 | 0.98 | 0.90 | 0.95 | 0.94 |
| HONO | FT | 1.02 | 1.45 | 1.10 | 1.02 | 1.03 | 1.04 |
| | blend | 1.20 | 1.17 | 1.16 | 1.00 | 1.02 | 1.03 |

A weak fuel-type dependence was observed for $NO_x$, which on average exhibited lower EI values during FT and FT-blend versus JP-8 fuel combustion experiments (Table 2). This is consistent with measurements made near engine exit at AAFEX and in a previous study in which $NO_x$ EI values were 5−11% lower in FT-derived exhaust.[12,32] Table 2 summarizes the JP-8 normalized emission indices of $NO_x$ and HONO for FT/FT-blend experiments. Note that a bias is introduced for these experiments because a constant, fuel-type independent $EI_{CO_2}$ value is used, since we do not know the relative contribution of exhaust from each engine measured at 145 m. This can account for at most 2% of the EI difference in the extreme case that exhaust from only the "experiment" engine was sampled during FT experiments. Moreover, we at times observe lower $NO_x$ EI for FT-blend than FT-only experiments, though we expect FT-blend values to be an average of the JP-8 and FT.[12] Ambient conditions that affect engine chemistry and measurement downstream including temperature, humidity, sunlight, transport time from emission to sampling, and the extent of the mixing of exhaust from the two engines could not be adjusted in a controlled manner, complicating direct comparisons between experiments.

HONO showed a fuel-type dependence opposite to that of $NO_x$ (Table 2), which cannot be attributed to the use of a constant $EI_{CO_2}$. Timko et al.[12] observed lower NO and higher $NO_2$ EI in FT-derived plumes compared to those utilizing only JP-8 fuel. That $NO_2$ and HONO, both byproducts of reactions involving NO, exhibit a fuel-type dependence trend that is opposite to that of NO indicates an environment that is more favorable to oxidation during FT-fuel combustion, perhaps a result of the absence of aromatics and sulfur compounds. Future experiments with speciated measurements of individual nitrogen oxide species under identical ambient conditions are required to determine whether the total amount of $NO_y$ produced or only the partitioning between species is affected by the use of synthetic fuels.

$NO_x$ EI exhibit a positive dependence on ambient temperature ($0.19 \pm 0.04$ g $kg^{-1}$ $K^{-1}$) at the maximum rated engine thrust (Supporting Information, Figure S2), consistent with the ICAO database.[33] A temperature dependence for HONO was not observed (Supporting Information, Figure S2), suggesting the chemical processes governing HONO production and loss are not sensitive to ambient temperatures.

**3.2. Comparison to Previous Campaigns.** HONO EI trend with increasing engine power observed during AAFEX is consistent with those from previous field campaigns.[23,34] Figure 4 shows good agreement at low engine power between HONO EI from AAFEX to those observed at the APEX-3 (using corrected line strengths), during which HONO was measured 1 m behind engine exit.[23] HONO EI from APEX-3 was lower by a factor of approximately three at higher engine thrust. The discrepancy may simply be explained by difference in engine type and age, both of which can influence aircraft $NO_x$ emissions.[35] However, because results agree well under some engine conditions but not others (Figure 4), a more likely explanation is incomplete HONO formation during APEX-3. Tremmel et al.[6] simulate HONO formation via R1 continuing for several milliseconds following engine exit; therefore, at higher engine power (i.e., higher exhaust velocity), HONO formation may not be complete at a distance of 1 m downstream as the remaining OH is quenched by the inlet probe. Consequently, HONO measured at 1 m may underestimate total production, suggesting sampling of reactive gases should be conducted farther downstream to ensure completion. Metal probes used to sample hot exhaust near engine exit and heating/dilution to prevent condensation in inlet lines during APEX-3 may have promoted HONO surface losses or thermal dissociation leading to underestimation of HONO.

Figure 3d shows HONO to $NO_x$ ratios observed during AAFEX ranging from 3 to 6%, which is consistent with predicted value of 4.5% in jet engine exhaust[30] and considerably higher than 0.29−0.8% reported for on-road vehicles, with diesel-powered engines emitting a higher ratio than their gasoline-powered counterparts.[36,37] Sampling exhaust from a diesel-powered generator during AAFEX revealed HONO/$NO_x$ of 0.82 ± 0.05% (Supporting Information, Figure S3). Lastly, recent measurements of exhaust from eight different commercial aircraft in flight[38] show decreasing HONO/$NO_y$ with increasing $NO_x$ EI, as also observed during AAFEX for engine settings simulating cruise conditions (~65% maximum rated engine thrust) and beyond.

**3.3. $H_2O_2$ Chemistry.** Hydrogen peroxide was detected in aircraft exhaust only at low/idle engine power. $H_2O_2$ EI for JP-8 fuel at low power (4%) is 0.34 ± 0.19 (1$\sigma$) g per kg fuel and decreases to below detection limit beyond 30% of maximum rated engine thrust. EI for $H_2O_2$ exhibits no dependence on ambient temperature. During combustion, $H_2O_2$ can be formed by the self-reactions of $HO_2$ (R5) and OH (R6). The $H_2O_2$ EI trend with respect to rated engine thrust reflects that of $NO_2$ (Figure 4), which Wood et al.[23] proposed is primarily generated during combustion by reaction involving $HO_2$ (R7) and exhibits the opposite trend of HONO, formed primarily by reaction involving OH (R1). Therefore, $HO_2$ by reaction R6 and not OH by reaction R5 is the likely $H_2O_2$ precursor in jet-fuel combustion. $HO_2$ is likely formed from the OH-driven oxidation of incomplete combustion byproducts such as carbon monoxide and formaldehyde, both of which exhibit EI trends similar to that of $H_2O_2$:[39]

$$OH + OH + M \rightarrow H_2O_2 \quad (R_5)$$

$$HO_2 + HO_2 + M \rightarrow H_2O_2 + O_2 \quad (R_6)$$

$$HO_2 + NO \rightarrow NO_2 + OH \quad (R_7)$$

Identification of $H_2O_2$ at levels comparable to those of HONO (Figure 2) at low engine thrust represents an additional airport-related source of $HO_x$ precursors to the boundary layer, though given its slow rate of photolysis and loss via deposition its impact on the $HO_x$ budget is likely to be much smaller than that of HONO. Though this was the first spectroscopic measurement of $H_2O_2$ in aircraft exhaust, the reported values for $H_2O_2$ from AAFEX should be qualified because of the yet uncharacterized potential for attenuation during sampling.

**3.4. Impact on Atmospheric Chemistry.** Emission indices of HONO observed during AAFEX are higher than those previously reported.[23,34] We calculate photolysis of idle-aircraft-emitted HONO at engine exit will yield OH at a rate of about 1000 ppt $s^{-1}$, which is roughly 3 orders of magnitude faster than observed in a typical sunny urban atmosphere. With increasing engine power (at higher altitudes), HONO goes from a dominant to nearly sole source of $HO_x$ in jet exhaust,[40] which can influence photochemistry in heavily traveled flight corridors. Consequently, $HO_x$ precursors emitted simultaneously with pollutants of interest should be included in models aimed at understanding the evolution of plumes from emission sources, particularly given the nonlinearity and cycling of $NO_x$−$HO_x$ chemistry prior to termination. Moreover, reported discrepancies on the potential significance of ClNO production,[41−43] a driver of catalytic stratospheric ozone destruction, due to HONO and HCl uptake on the surface of $H_2SO_4$ aerosols require more information of, among other variables, HONO levels in aircraft exhaust. This study characterizing emission indices as a function of engine power, ambient conditions and fuel-type, in addition to gaining insight into engine chemistry, provides a useful tool for such applications.

## ■ ASSOCIATED CONTENT

**Supporting Information.** Figures showing (1) the response times of HONO and $CH_4$ during a standard addition test in the field at the end of the AAFEX campaign, (2) temperature dependence of $NO_x$ and HONO emission indices at high engine power, and (3) the HONO to $NO_x$ ratio measured in diesel-generated exhaust at AAFEX. This information is available free of charge via the Internet at http://pubs.acs.org/

## ■ AUTHOR INFORMATION

**Corresponding Author**
*Phone: (617) 496-6246; e-mail: hwanlee@fas.harvard.edu.

**Present Addresses**
§Current address: University of Massachusetts, Department of Public Health, Amherst, MA 01003, United States.

## ■ ACKNOWLEDGMENT

This research was supported in part by the National Science Foundation (Award Nos. AGS 0813617 and 0814202). The authors gratefully acknowledge W. Berk Knighton of Montana State University, Michael T. Timko and Zhenhong Yu of Aerodyne Research, Inc., Bruce E. Anderson of NASA Langley Research Center, and all of the support staff and scientists of the AAFEX team.

## ■ REFERENCES

(1) Brasseur, G. P.; Cox, R. A.; Hauglustaine, D. I. I.; Lelieveld, J.; Lister, D. H.; Sausen, R.; Schumann, U.; Wahner, A.; Wiesen, P. European

scientific assessment of the atmospheric effects of aircraft emissions. *Atmos. Environ.* **1998**, *32* (13), 2329–2418.

(2) National Research Council (U.S.). Panel on Atmospheric Effects of Aviation. *Atmospheric effects of aviation: a review of NASA's subsonic assessment project*; National Academy Press: Washington, D.C., 1999; p xii, p 41.

(3) National Research Council (U.S.). Panel on Atmospheric Effects of Aviation. *A review of NASA's atmospheric effects of stratospheric aircraft project*; National Academy Press: Washington, D.C., 1999; p ix, p 50.

(4) Toohey, D.; McConnell, J.; Avallone, L.; Evans, W. Aviation and chemistry and transport processes in the upper troposphere and lower stratosphere. *Bull. Am. Meteorol. Soc.* **2010**, *91* (4), 485.

(5) Beier, K.; Schreier, F. Modeling of aircraft exhaust emissions and infrared-spectra for remote measurement of nitrogen-oxides. *Ann. Geophys.* **1994**, *12* (10−11), 920–943.

(6) Tremmel, H. G.; Schlager, H.; Konopka, P.; Schulte, P.; Arnold, F.; Klemm, M.; Droste-Franke, B. Observations and model calculations of jet aircraft exhaust products at cruise altitude and inferred initial OH emissions. *J. Geophys. Res., [Atmos.]* **1998**, *103* (D9), 10803–10816.

(7) Sovde, O. A.; Gauss, M.; Isaksen, I. S. A.; Pitari, G.; Marizy, C. Aircraft pollution - a futuristic view. *Atmos. Chem. Phys.* **2007**, *7* (13), 3621–3632.

(8) Tesseraux, I. Risk factors of jet fuel combustion products. *Toxicol. Lett.* **2004**, *149* (1−3), 295–300.

(9) Jarvis, D. L.; Leaderer, B. P.; Chinn, S.; Burney, P. G. Indoor nitrous acid and respiratory symptoms and lung function in adults. *Thorax* **2005**, *60* (6), 474–479.

(10) Pitts, J. N.; Grosjean, D.; Vancauwenberghe, K.; Schmid, J. P.; Fitz, D. R. Photo-oxidation of aliphatic-amines under simulated atmospheric conditions - formation of nitrosamines, nitramines, amides, and photo-chemical oxidant. *Environ. Sci. Technol.* **1978**, *12* (8), 946–953.

(11) Sleiman, M.; Gundel, L. A.; Pankow, J. F.; Jacob, P.; Singer, B. C.; Destaillats, H. Formation of carcinogens indoors by surface-mediated reactions of nicotine with nitrous acid, leading to potential thirdhand smoke hazards. *Proc. Natl. Acad. Sci. U.S.A.* **2010**, *107* (15), 6576–6581.

(12) Timko, M. T.; Yu, Z.; Onasch, T. B.; Wong, H. W.; Miake-Lye, R. C.; Beyersdorf, A. J.; Anderson, B. E.; Thornhill, K. L.; Winstead, E. L.; Corporan, E.; DeWitt, M. J.; Klingshirn, C. D.; Wey, C.; Tacina, K.; Liscinsky, D. S.; Howard, R.; Bhargava, A. Particulate emissions of gas turbine engine combustion of a Fischer−Tropsch synthetic fuel. *Energy Fuels* **2010**, *24*, 5883–5896.

(13) Miller, D. L.; Lenhert, D. B.; Cernansky, N. P. The oxidation of JP-8, Jet-A, and their surrogates in the low and intermediate temperature regime at elevated pressures. *Combust. Sci. Technol.* **2007**, *179* (5), 845–861.

(14) Bulzan, D.; Anderson, B.; Wey, C.; Howard, R.; Winstead, E. H.; Beyersdorf, A.; Corporan, E.; DeWitt, M. J.; Klingshirn, C. D.; Herndon, S. C.; Miake-Lye, R.; Wood, E. C.; Tacina, K.; Liscinsky, D. S.; Hagen, D.; Lobo, P.; Whitefield, P. In *Gaseous and Particulate Emissions Results of the NASA Alternative Aviation Fuel Experiment (AAFEX)*; ASME Turbo Expo 2010: Power for Land, Sea, and Air (GT2010): Glasgow, U.K., 2010; pp 1195−1207.

(15) Lee, B. H.; Wood, E. C.; Zahniser, M. S.; McManus, J. B.; Nelson, D. D.; Herndon, S. C.; Santoni, G. W.; Wofsy, S. C.; Munger, J. W. Simultaneous measurements of atmospheric HONO and NO2 via absorption spectroscopy using tunable mid-infrared continuous-wave quantum cascade lasers. *Appl. Phys. B* **2011**, *102* (2), 417–423.

(16) Santoni, G. W.; Lee, B. H.; Wood, E. C.; Herndon, S. C.; Miake-Lye, R. C.; Wofsy, S. C.; McManus, J. B.; Nelson, D. D.; Zahniser, M. S. Aircraft emissions of methane and nitrous oxide during the alternative aviation fuel experiment. *Environ. Sci. Technol.* **2011**accepted for publication.

(17) Becker, K. H.; Kleffmann, J.; Kurtenbach, R.; Wiesen, P. Solubility of nitrous acid (HONO) in sulfuric acid solutions. *J. Phys. Chem.* **1996**, *100* (36), 14984–14990.

(18) OSullivan, D. W.; Lee, M. Y.; Noone, B. C.; Heikes, B. G. Henry's law constant determinations for hydrogen peroxide, methyl hydroperoxide, hydroxymethyl hydroperoxide, ethyl hydroperoxide, and peroxyacetic acid. *J. Phys. Chem.* **1996**, *100* (8), 3241–3247.

(19) Guilmot, J. M.; Godefroid, M.; Herman, M. Rovibrational parameters for trans-nitrous acid. *J. Mol. Spectrosc.* **1993**, *160* (2), 387–400.

(20) Guilmot, J. M.; Melen, F.; Herman, M. Rovibrational parameters for cis-nitrous acid. *J. Mol. Spectrosc.* **1993**, *160* (2), 401–410.

(21) Melen, F.; Herman, M. Vibrational bands of hxnyoz molecules. *J. Phys. Chem. Ref. Data* **1992**, *21* (4), 831–881.

(22) Nelson, D. D.; Shorter, J. H.; McManus, J. B.; Zahniser, M. S. Sub-part-per-billion detection of nitric oxide in air using a thermoelectrically cooled mid-infrared quantum cascade laser spectrometer. *Appl. Phys. B* **2002**, *75* (2−3), 343–350.

(23) Wood, E. C.; Herndon, S. C.; Timko, M. T.; Yelvington, P. E.; Miake-Lye, R. C. Speciation and chemical evolution of nitrogen oxides in aircraft exhaust near airports. *Environ. Sci. Technol.* **2008**, *42* (6), 1884–1891.

(24) Rothman, L. S.; Gordon, I. E.; Barbe, A.; Benner, D. C.; Bernath, P. E.; Birk, M.; Boudon, V.; Brown, L. R.; Campargue, A.; Champion, J. P.; Chance, K.; Coudert, L. H.; Dana, V.; Devi, V. M.; Fally, S.; Flaud, J. M.; Gamache, R. R.; Goldman, A.; Jacquemart, D.; Kleiner, I.; Lacome, N.; Lafferty, W. J.; Mandin, J. Y.; Massie, S. T.; Mikhailenko, S. N.; Miller, C. E.; Moazzen-Ahmadi, N.; Naumenko, O. V.; Nikitin, A. V.; Orphal, J.; Perevalov, V. I.; Perrin, A.; Predoi-Cross, A.; Rinsland, C. P.; Rotger, M.; Simeckova, M.; Smith, M. A. H.; Sung, K.; Tashkun, S. A.; Tennyson, J.; Toth, R. A.; Vandaele, A. C.; Vander Auwera, J. The HITRAN 2008 molecular spectroscopic database. *J. Quant. Spectrosc. Radiat. Transfer* **2009**, *110* (9−10), 533–572.

(25) Herndon, S. C.; Shorter, J. H.; Zahniser, M. S.; Nelson, D. D.; Jayne, J.; Brown, R. C.; Miake-Lye, R. C.; Waitz, I.; Silva, P.; Lanni, T.; Demerjian, K.; Kolb, C. E. NO and $NO_2$ emission ratios measured from in-use commercial aircraft during taxi and takeoff. *Environ. Sci. Technol.* **2004**, *38* (22), 6078–6084.

(26) Lavoie, G. A. Spectroscopic measurements of nitric oxide in spark ignition engines. *Combust. Flame* **1970**, *15* (2), 97–&.

(27) Mebel, A. M.; Lin, M. C.; Melius, C. F. Rate constant of the HONO+HONO -> $H_2O$+NO+$NO_2$ reaction from ab initio MO and TST calculations. *J. Phys. Chem. A* **1998**, *102* (10), 1803–1807.

(28) Xia, W. S.; Lin, M. C. Ab initio MO/statistical theory prediction of the OH plus HONO reaction rate: evidence for the negative temperature dependence. *PhysChemComm* **2000**, *3*, 71–78.

(29) Bockle, S.; Einecke, S.; Hildenbrand, F.; Orlemann, C.; Schulz, C.; Wolfrum, J.; Sick, V. Laser-spectroscopic investigation of OH-radical concentrations in the exhaust plane of jet engines. *Geophys. Res. Lett.* **1999**, *26* (13), 1849–1852.

(30) Garnier, F.; Baudoin, C.; Woods, P.; Louisnard, N. Engine emission alteration in the near field of an aircraft. *Atmos. Environ.* **1997**, *31* (12), 1767–1781.

(31) Brown, L. R.; Farmer, C. B.; Rinsland, C. P.; Toth, R. A. Molecular line parameters for the atmospheric trace molecule spectroscopy experiment. *Appl. Opt.* **1987**, *26* (23), 5154–5182.

(32) Timko, M. T.; Herndon, S. C.; De la Rosa Blanco, E.; Wood, E. C.; Yu, Z.; Miake-Lye, R. C.; Knighton, W. B. Combustion products of jet fuel, Fischer−Tropsch synthetic fuel, and biomass jet fuel for a gas turbine engine. *Combust. Sci. Technol.* **2011**publication in review.

(33) DuBois, D.; Paynter, G. C., Fuel flow method2 for estimating aircraft emissions. *Soc. Automot. Eng.* **2006**.

(34) Wormhoudt, J.; Herndon, S. C.; Yelvington, P. E.; Miake-Lye, R. C.; Wey, C. Nitrogen oxide ($NO/NO_2$/HONO) emissions measurements in aircraft exhausts. *J. Propul. Power* **2007**, *23* (5), 906–911.

(35) Lukachko, S. P.; Waitz, I. A. Effects of engine aging on aircraft NOx emissions. In *International Gas Turbine & Aeroengine Congress & Exhibition*;Engineers, A. S. o. M., Ed.; Orlando, FL, 1997.

(36) Kirchstetter, T. W.; Harley, R. A.; Littlejohn, D. Measurement of nitrous acid in motor vehicle exhaust. *Environ. Sci. Technol.* **1996**, *30* (9), 2843–2849.

(37) Kurtenbach, R.; Becker, K. H.; Gomes, J. A. G.; Kleffmann, J.; Lorzer, J. C.; Spittler, M.; Wiesen, P.; Ackermann, R.; Geyer, A.; Platt, U.

Investigations of emissions and heterogeneous formation of HONO in a road traffic tunnel. *Atmos. Environ.* **2001**, 35 (20), 3385–3394.

(38) Jurkat, T.; Voigt, C.; Arnold, F.; Schlager, H.; Kleffmann, J.; Aufmhoff, H.; Schauble, D.; Schaefer, M.; Schumann, U. Measurements of HONO, NO, NO(y) and SO(2) in aircraft exhaust plumes at cruise. *Geophys. Res. Lett.* **2011**, 38.

(39) Yelvington, P. E.; Herndon, S. C.; Wormhoudt, J. C.; Jayne, J. T.; Miake-Lye, R. C.; Knighton, W. B.; Wey, C. Chemical speciation of hydrocarbon emissions from a commercial aircraft engine. *J. Propul. Power* **2007**, *23* (5), 912–918.

(40) Wood, E. C.; Herndon, S. C.; Timko, M. T.; Yu, Z.; Miake-Lye, R. C.; Lee, B. H.; Santoni, G. W.; Wofsy, S. C.; Munger, J. W.; Knighton, W. B.; Anderson, B. Aircraft emissions, plume chemistry, and alternative fuels: results from the APEX and AAFEX campaigns. *American Geophysical Union Meeting*; AGU: San Francisco, CA, 2009.

(41) Fenter, F. F.; Rossi, M. J. Heterogeneous kinetics of HONO on $H_2SO_4$ solutions and on ice: Activation of HCl. *J. Phys. Chem.* **1996**, *100* (32), 13765–13775.

(42) Longfellow, C. A.; Imamura, T.; Ravishankara, A. R.; Hanson, D. R. HONO solubility and heterogeneous reactivity on sulfuric acid surfaces. *J. Phys. Chem. A* **1998**, *102* (19), 3323–3332.

(43) Zhang, R. Y.; Leu, M. T.; Keyser, L. F. Heterogeneous chemistry of HONO on liquid sulfuric acid: A new mechanism of chlorine activation on stratospheric sulfate aerosols. *J. Phys. Chem.* **1996**, *100* (1), 339–345.